Journal of Alloys and Compounds 509 (2011) 2277–2284

Contents lists available at ScienceDirect

Journal of Alloys and Compounds

journal homepage: www.elsevier.com/locate/jallcom

Phase abundances in AB_2 metal hydride alloys and their correlations to various properties

K. Young [a,*], J. Nei [b], T. Ouchi [a], M.A. Fetcenko [a]

[a] Energy Conversion Devices Inc./Ovonic Battery Company, 2983 Waterview Drive, Rochester Hills, MI 48309, USA
[b] Department of Chemical Engineering, Wayne State University, Detroit, MI 48302, USA

ARTICLE INFO

Article history:
Received 26 August 2010
Received in revised form 1 November 2010
Accepted 2 November 2010
Available online 10 November 2010

Keywords:
Hydrogen absorbing materials
Transition metal alloys
Metal hydride electrode
Electrochemical reactions

ABSTRACT

The phase abundances of 16 alloys with various contents of Sn, Co, Al, and Fe additives were studied by X-ray diffraction analysis. Due to relative small percentages, the relative abundances of these minor phases were obtained through smoothing, curve fitting, and area integration and correlated qualitatively to the amount of additives in the alloys. In the Laves phases, Sn, Co, and Fe with more outer-shell electrons than that of the host alloy promote C15 phase. Al, with less outer-shell electrons, on the other hand, promotes C14 phase. In the AB phases, Sn promotes the formation of ZrNi phase and suppresses the formation of TiNi phase. In the competition between Zr_7Ni_{10} and Zr_9Ni_{11} (both are the products from a solid-state transformation), Sn promotes Zr_7Ni_{10} while both Fe and Al promote Zr_9Ni_{11}. The phase abundances were further correlated to the gas phase and electrochemical properties of the alloys. C14, Zr_9Ni_{11}, and TiNi phases were found to increase both the gas phase and electrochemical storage capacities, lower the hydrogen equilibrium pressure, decrease the half-cell high-rate dischargeability, improve both charge retention and cycle life, and slightly decrease the capacity recovery after storing at 45 °C for 60 days. C15, ZrNi, and Zr_7Ni_{10} phases work in the opposite manner.

1. Introduction

Laves phase AB_2 alloys are strong candidates to replace mischmetal based AB_5 alloys used as metal hydride (MH) electrode in nickel metal hydride (Ni/MH) battery due to their higher storage capacity and flexibility in composition design [1–22]. The AB_2 alloys suitable for the Ni/MH application are multi-phased with the main phase consisting of C14, C15, or both Laves phases and one or more secondary phases including TiNi, Zr_7Ni_{10}, Zr_9Ni_{11}, ZrNi, or BCC-structured non-Laves phases [23–29]. Although the microstructure and solidification path of these complicated AB_2 MH alloys have been studied [30,31], reports on the contribution of each phase to the electrochemical properties are very limited [32,33]. Most of the comparisons were based on varying composition to alter the C14/C15 phase abundance and therefore the contribution of composition cannot be eliminated from the conclusion [34–38]. Our previous report was able to isolate the contribution from C14/C15 abundance by comparing the microstructures and properties of three alloys before and after annealing [21]. The C15 structure was found to have higher hydrogen storage capacity and reversibility in gas phase hydrogen storage, and better high-rate dischargeability (HRD), hydrogen bulk diffusion, specific power, and low temperature performance with a shortcoming of inferior electrochemical cycle life. The contribution from secondary phases as a whole was also studied in the same paper by comparing the properties before and after the annealing process. After annealing, most of the secondary phases were eliminated and the electrochemical properties deteriorated, as reported by Visintin et al. previously [39]. These non-Laves Zr_xNi_y secondary phases as a group were found to play an importance role in the activation, rate capability, charge retention, and cycle life of Ni/MH battery. Changes in the electrochemical properties of AB_5 compounds due to annealing were also reported recently [40–42]. The function of each non-Laves phase is not clear and will be discussed in this paper.

2. Experimental setup

The sample preparation, gas phase characteristic measurement, half-cell testing, and sealed-cell assembly and testing have been described in a previous publication [16]. In this report, a new set of samples were prepared by arc melting for the X-ray diffraction (XRD) study. The microstructures of the samples made by induction melting and arc melting have been compared previously and the results are very close to each other [8]. A Rigaku Miniflex XRD was used to study the microstructure. The phase abundances of secondary phases were estimated by comparing the integration of XRD intensities over the characteristic deflection peak regions.

3. Results and discussion

Designed with a modified L-16 orthogonal array, 16 alloys with the general formula $Ti_9Zr_{27-w}V_5Ni_{38}Cr_{5-x}Mn_{16-y-z}Sn_wCo_xAl_yFe_z$ were prepared to study the effects of Sn, Co, Al, and Fe as additives to the C14/C15 mixed Laves phase alloy in Ni/MH battery [16].

* Corresponding author. Tel.: +1 248 293 7000; fax: +1 248 299 4520.
E-mail addresses: kyoung@ovonic.com, kwoyoung@yahoo.com (K. Young).

0925-8388/$ – see front matter © 2010 Elsevier B.V. All rights reserved.
doi:10.1016/j.jallcom.2010.11.005

Table 1
a and *c* lattice constants of C14 and phase abundances in % found from XRD analysis.

Alloy #	*a* (in Å)	*c* (in Å)	C14	C15	ZrNi	TiNi	Zr_7Ni_{10}	Zr_9Ni_{11}	Total secondary phases
1	5.0032	8.1693	81.6	16.8	0.09	0.63	0.37	0.49	1.59
2	4.9995	8.1621	71.2	27.2	0.08	0.52	0.32	0.68	1.61
3	5.0019	8.1633	70.8	26.9	0.13	1.00	0.30	0.86	2.30
4	5.0008	8.1622	71.2	27.1	0.11	0.56	0.23	0.77	1.67
5	5.0018	8.1589	68.3	30.1	0.20	0.45	0.30	0.63	1.58
6	4.9991	8.1596	60.3	38.2	0.08	0.53	0.30	0.55	1.47
7	5.0031	8.1655	69.4	29.5	0.14	0.39	0.26	0.34	1.13
8	4.9982	8.1562	58.6	40.0	0.15	0.51	0.33	0.40	1.39
9	4.9983	8.1568	73.3	24.7	0.14	0.59	0.40	0.87	1.99
10	5.0024	8.1655	74.0	24.4	0.18	0.53	0.29	0.64	1.64
11	4.9997	8.1646	49.3	49.4	0.19	0.54	0.38	0.14	1.26
12	4.9952	8.1577	56.2	42.3	0.23	0.51	0.39	0.42	1.55
13	5.0047	8.1629	71.0	27.4	0.24	0.46	0.54	0.38	1.61
14	4.9982	8.1659	68.7	29.7	0.33	0.43	0.60	0.24	1.60
15	4.9964	8.1577	49.8	49.0	0.24	0.30	0.45	0.18	1.17
16	4.9945	8.1551	42.9	55.7	0.18	0.36	0.60	0.23	1.37

Orthogonal arrays are designed to reduce the number of experiments while still being capable of obtaining statistically relevant conclusions. In this design of experiments, we only need 16 alloys instead of the full matrix of 256 alloys with four variables at four levels each. The designed composition, gas phase storage, and electrochemical properties of these alloys are summarized in Table 1 and Table 4 of Ref. [16].

3.1. XRD phase analysis

The XRD spectra ranging from 30 to 60° 2θ for alloy #1 to #16 prepared by arc melting are shown in Figs. 1a and 2a. The lattice constants *a* and *c* of C14 structure were calculated from the XRD spectra and are listed in Table 1. The C14 and C15 phase abundances were calculated from the integration of diffraction peaks using a calibration with previous samples done by Rietveld method. The results of C14 abundance are shown in Table 1. The C14 phase abundance correlates very well with the average electron density (*e*/*a*), as shown in Fig. 3. A transition threshold of approximately 6.95 is observed, which agrees well with previous reports [43,44].

In order to identify and quantify the secondary phases, 2θ range from 35 to 45° in each XRD spectrum was expanded and illustrated in Figs. 1b and 2b. The major diffraction peak profiles of these secondary phases were processed (smoothing, curve fitting, and area integration) and used to estimate the phase abundances as listed in Table 1. Without a cross-calibration with a second phase analysis, the phase abundances reported here are only for comparison purpose and may be different from the actual value.

3.2. Correlation between phase abundance and chemical composition

The C14 phase abundance is plotted against the amount of various additives in Fig. 4a. Each data point was obtained by averaging the four values of C14 phase abundance from the corresponding alloys with a specific amount of a particular additive. The general trends of all correlations are in agreement with the prediction from *e*/*a* values. Sn, Co, and Fe have more outer-shell electrons than the *e*/*a* values of the alloys (about 7) and consequently lower the C14 phase abundance, and Al with less outer-shell electrons (3) has the opposite effect. Since the total non-Laves secondary phase abundances (Table 1) are small and vary in a narrow range (most are within 1 and 2%), the trends of C15 phase abundance dependency on composition variation are contrary to those of C14. Same trends of C15 phase abundance as functions of Fe, Co, and Al can also be found in a series of Zr_7Ni_{10}-based quinary alloys [44].

There are two AB phases observed in the XRD analysis. One has a lattice parameter about that of ZrNi crystal structure, and the other one's is close to that of TiNi crystal structure. The former was found to follow the phase evolution from ZrNi + Zr_9Ni_{11} to Zr_9Ni_{11}, Zr_9Ni_{11} + Zr_7Ni_{10}, and finally Zr_7Ni_{10} [44]. The ZrNi phase, with a B33 (CrB) structure [45], was never found to coexist with Zr_7Ni_{10} through composition variation [44,46–49]. It is possibly a remnant of the precursor material for the consequent solid transformation into Zr_9Ni_{11} and Zr_7Ni_{10} phases [30]. B2 and B33 structures are related. With increasing level of Co substituting Ni in ZrNi alloy, the B33 phase changes into B2 phase [45]. TiNi may be one of the products of solid phase transformation, which forms an alternative band structure with Zr_7Ni_{10} phase as observed from Fig. 16a in Ref. [31]. With the Zr/Ti content at 21.5/12, only TiNi structure was found in the XRD analysis [18]. When the Zr/Ti content changes from 21.5/12 to 26/9, ZrNi phase starts to appear [16]. As the Zr/Ti content moves to 32.3/9, only ZrNi phase is found [32]. The lattice parameters of both AB phases indicate the occupancies of Zr and Ti in the A-sites. The fine structure of this group of alloys will be investigated by transition electron microscope and reported elsewhere. The ZrNi and TiNi phase abundances are plotted against the amount of additives in Fig. 4b and c, respectively. The only major correlation is from Sn additive. As more Sn is added into the alloy to substitute Zr, the ZrNi content increases almost linearly, and the general trend of TiNi phase abundance is decreasing. With reducing Zr-content in the alloy from 26.6 to 26.0 at.%, the amount of ZrTi increases while that of TiNi decreases. Sn may play a crucial role in determining which AB phase is to be formed.

Zr_7Ni_{10} phase was reported to have good hydrogen storage capability [23,50,51]. The structural and electrochemical properties of $Ti_xZr_{7-x}Ni_{10}$ alloys were reported before [52]. Its abundance is plotted against the content of additives in Fig. 4d. Higher Sn levels (0.6 and 0.8 at.%) increase the Zr_7Ni_{10} phase abundance by a large amount; however, higher Fe levels demonstrate the opposite results. The trends of Co and Al are less obvious. In the study of modifiers in Zr_7Ni_{10} based quinary alloys, Al, Co, and Fe were shown to reduce the phase abundance of Zr_7Ni_{10} in favor of Laves phases [44].

Zr_9Ni_{11} phase is a very good catalyst for hydrogen absorption/desorption [23,29]. Its abundance is plotted against the content of additives in Fig. 4e. The general trends with Sn, Fe, and Al are in the opposite direction to those of Zr_7Ni_{10}, and the trend with Co is identical to that of Zr_7Ni_{10}. Al and Fe promote Zr_9Ni_{11} while Co and Sn suppress it. As a comparison, Al, Co, and Fe in Zr_7Ni_{10} based quinary alloys were shown to first increase the Zr_9Ni_{11} phase abundance and then converge to a similar value (~35 at.%) at higher content of substitution [44].

The total non-Laves secondary phase abundance (ZrNi, TiNi, Zr_7Ni_{10}, and Zr_9Ni_{11}) is listed in Table 1 and plotted against the

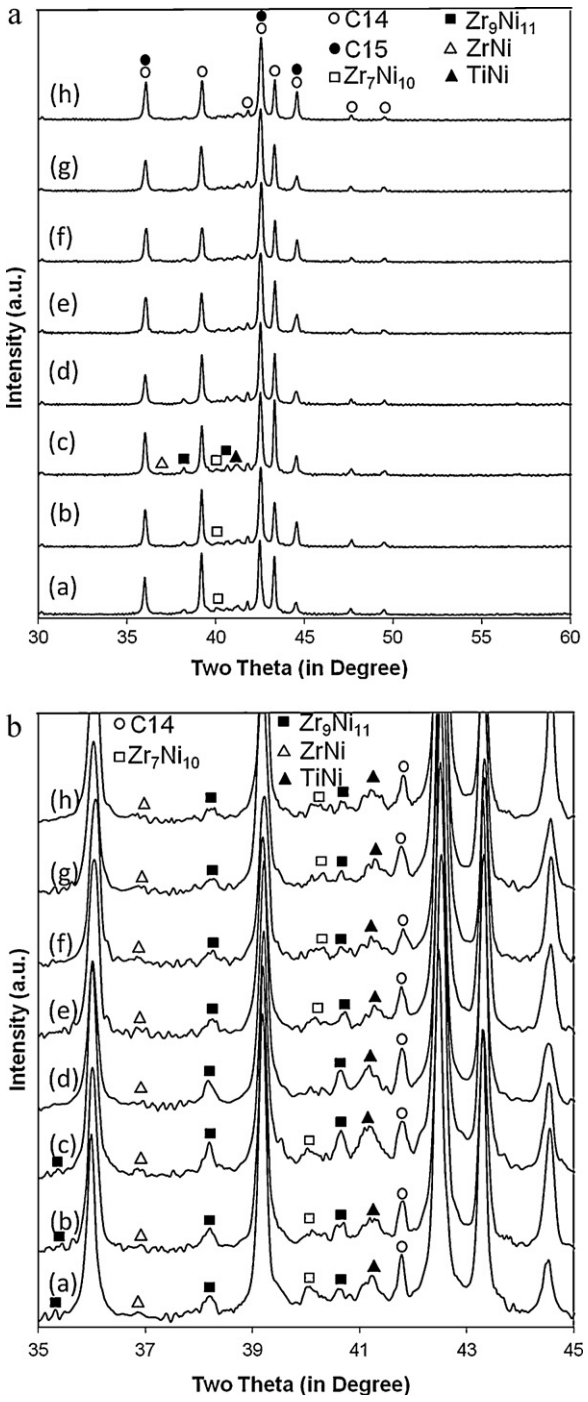

Fig. 1. XRD spectra using Cu-K_α as the radiation source for alloys #1 (a), #2 (b), #3 (c), #4 (d), 5 (e), #6 (f), #7 (g), and #8 (h). b is magnified from a to emphasize the secondary phases.

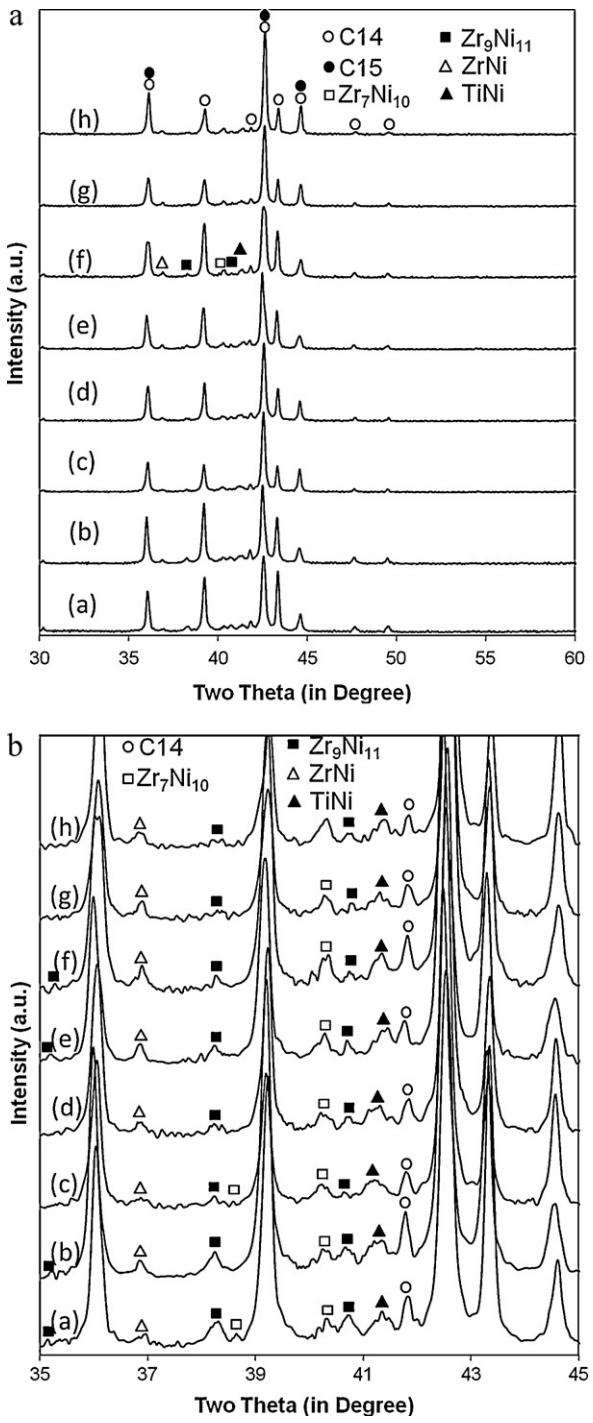

Fig. 2. XRD spectra using Cu-K_α as the radiation source for alloys #9 (a), #10 (b), #11 (c), #12 (d), 13 (e), #14 (f), #15 (g), and #16 (h). b is magnified from a to emphasize the secondary phases.

amount of additives in Fig. 4f. The trends with Al and Fe are similar: the total amount of secondary phases remains the same at lower level of substitution (0.4 at.%), increases by a large amount at the replacement level of 0.8 at.%, and then decreases when further increasing to 1.2 at.%. The trend with Co is decreasing in the beginning and stabilized afterward. The trend with Sn is not clear.

3.3. Correlation between phase abundance and properties

The correlations between various properties (both gas phase and electrochemical) of a series of Laves phase based AB_2 MH alloys to Ni, Cr, Mn, Sn, Co, and Al-content of were reported previously [11]. In this paper, the correlations of the same properties to the phase abundances of Laves main phases and the non-Laves secondary phases are discussed. The correlation factor (R^2) obtained from linear interpolations using Microsoft Excel are listed in Table 2. Higher R^2 values indicate a stronger correlation. The sign after each R^2 value in Table 2 indicates the direction of dependency. The positive sign is assigned to a positive correlation while the negative sign represents a negative correlation. Numbers in **bold** have values higher than 0.35 and are considered to be very significant.

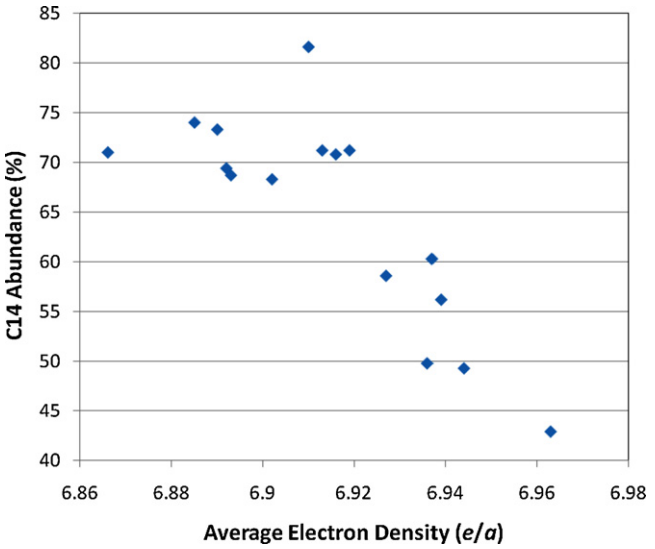

Fig. 3. The C14 phase abundance vs. the average electron density (e/a) of the alloys. A C14/C15 threshold was found at around $e/a = 6.95$.

Three gas phase properties are correlated to the phase abundances and the correlation factors are listed in the first three columns of Table 2. The maximum storage capacity correlates very strongly in the negative direction with the amount of ZrNi phase in the alloy (Fig. 5). As discussed in the section above, ZrNi is the precursor phase for the further solid-state transformation into Zr_7Ni_{10} and Zr_9Ni_{11} phases. A more complete transformation may be beneficial to the maximum storage capacity. Zr_7Ni_{10} phase is found to decrease the storage capacity. Two pressures were used to characterize the plateau position due to the nature of plateau region's larger slope in Ni-rich AB_2 alloys. Both pressures show the same trend in dependency on the abundance of each individual phase. While C14, Zr_9Ni_{11}, and TiNi phases reduce the plateau pressure, C15, Zr_7Ni_{10}, and ZrNi phases increase the plateau pressure (Figs. 6–8). However, in a previous study comparing AB_2 alloys before and after annealing, C15 phase was found to increase the hydrogen storage capacity [21]. Therefore, the conclusion reached before in Ref. [18] may be only applicable in a small composition range of these complicated multi-phase AB_2 alloys. Comparing to Zr_7Ni_{10}, pure Zr_9Ni_{11} has weaker metal-hydrogen bond strength and higher plateau pressure. However, in this case, their contributions to plateau pressure are opposite to the prediction from pure binary alloys. Compared to ZrNi, TiNi also has a weaker metal-hydrogen bond strength and is expected to raise the plateau pressure. Nevertheless, in our observation, TiNi phase reduces the plateau pressure and ZrNi raises it. With the complicated proximity effect among various phases, the behaviors of the phases are very different from those of the simple binary alloys.

The next three columns of Table 2 (4th–6th) summarize the correlation factors between the electrochemical properties measured from half-cell testing and phase abundances. Precharge is a measurement of the ease of activation and has been described before [12,17,18]. In this group of alloys, only C14 shows a negative impact to the ease of formation while contributions from other phases are negligible. In the case of discharge capacity, C14, TiNi, and Zr_9Ni_{11} contribute positively while C15, ZrNi, and Zr_7Ni_{10} have the opposite effect. The discharge capacity is plotted against the C14 phase abundance in Fig. 9, and a positive dependency is shown. The signs of the correlations of half-cell HRD are identical to those of PCT plateau pressure and are opposite to those of both gas phase and electrochemical storage capacities. Alloys with higher plateau pressure show better HRD in exchange for lower overall capacity.

Table 2
The correlation factors (R^2) between phase abundances and various gas phases and electrochemical properties of the alloys. Numbers in **bold** are significant. Plus (+) and minus (−) signs after the numbers indicate positive and negative correlations, respectively.

	Max gas phase storage (wt.%)	Mid-point pressure (MPa)	Pressure @ 1.1 wt.% (MPa)	Precharge (mAh/g)	Electrochemical discharge capacity (mAh/g)	Half-cell HRD@ 3rd cycle	Mid-point voltage (V)	Cap@2 C/Cap@0.5 C	Cap@ −10 °C	Charge retention after 30 days	Capacity recovery after 45 °C and 60 days	Specific power (W/kg)	Cycle life
C14	0.025+	**0.756**−	**0.580**−	0.166−	**0.384+**	0.139−	0.070+	0.009+	0.007−	0.194+	0.095−	0.009+	0.010+
ZrNi	**0.695**−	0.034+	**0.386+**	0.062+	0.217−	0.313+	0.000	0.003−	0.005−	0.232−	0.041+	0.000+	**0.373**−
TiNi	0.109+	0.209−	0.227−	0.002+	0.215+	0.075−	0.064+	0.066+	0.048+	0.227+	0.073−	0.010+	0.170+
Zr_7Ni_{10}	0.218−	0.094+	0.341+	0.024+	0.251−	0.300+	0.001−	0.186−	0.007+	0.327−	0.006+	0.002+	0.257−
Zr_9Ni_{11}	0.075+	0.288−	0.324−	0.021−	0.350+	0.243−	0.000−	0.028+	0.058−	**0.472+**	0.191−	0.008+	0.116+
Total secondary	0.000	0.269−	0.117−	0.001+	0.179+	0.040−	0.015+	0.008+	0.004−	0.227+	0.178−	0.023+	0.024+

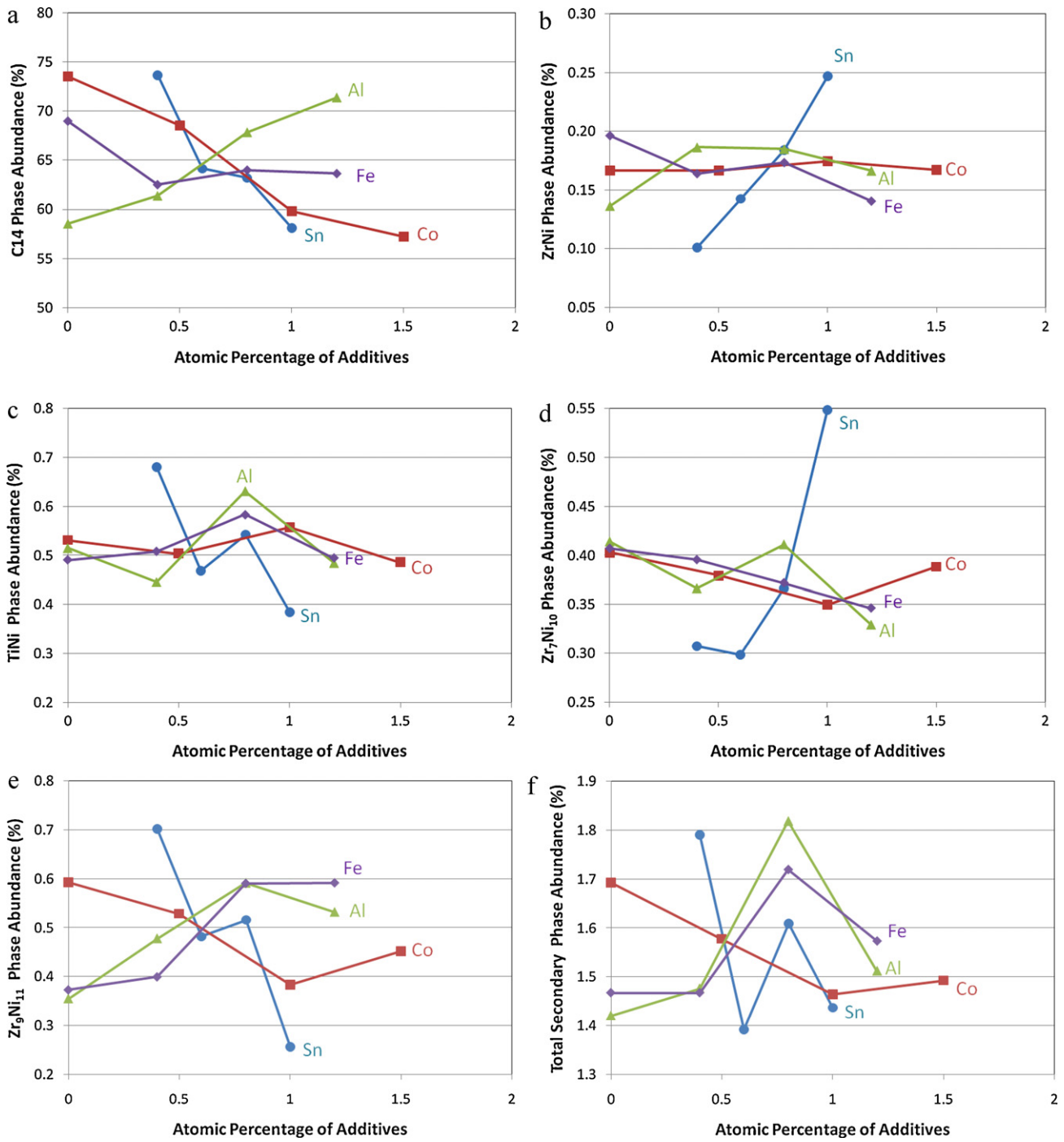

Fig. 4. The phase abundance of C14 (a), ZrNi (b), TiNi (c), Zr_7Ni_{10} (d), Zr_9Ni_{11} (e), and the sum of all secondary phases (f) vs. the amount of additives including Sn, Co, Al, and Fe.

The last seven columns of Table 2 (7th–13th) list the correlations of various Ni/MH battery performance characteristics to phase abundance. While most of the correlation factors are small, charge retention and cycle life are the two properties which have some stronger correlations to phase abundance. C14, TiNi, and Zr_9Ni_{11} enhance charge retention while C15, ZrNi, and Zr_7Ni_{10} act oppositely. The positive correlation between charge retention and Zr_9Ni_{11} phase abundance is shown in Fig. 10. In the cycle life category, C14, TiNi, and Zr_9Ni_{11} are beneficial while C15, ZrNi, and Zr_7Ni_{10} are detrimental. Similar cycle life advantage of C14 over C15 phase was reported before [21]. The negative correlation of cycle life vs. ZrNi phase abundance is shown in Fig. 11. One other result worth mentioning here is the sealed-cell HRD, defined by the ratio of capacities obtained from 2 C and 0.5 C discharge rates. The correlations are weak but the signs are totally opposite to those in half-cell HRD. Both the abundant amount of electrolyte and lower hydrogen pressure in a half-cell configuration may contribute to different electrochemical results comparing to sealed-cell one. In the sealed cell, the surface of MH electrode is semi-starved of electrolyte, causing a deficiency of hydroxide ions near the surface which will recombine with proton from the discharged MH electrode. In this case, the thickness, porosity, and shape of tunnels in the surface oxide play important role in the half-cell HRD measurement, but not in a half-cell configura-

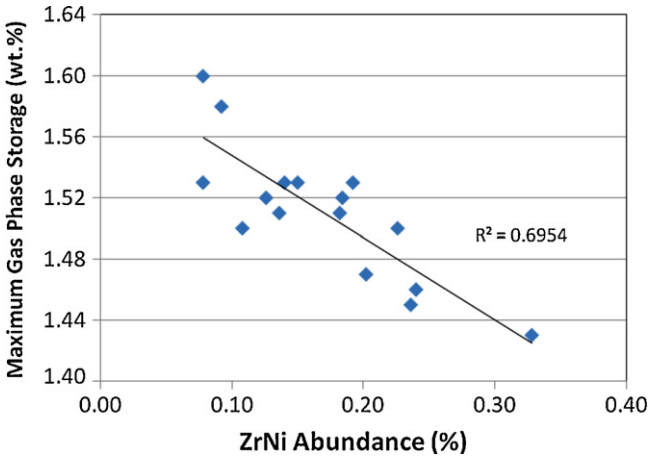

Fig. 5. Maximum gas phase storage capacity from PCT analysis vs. ZrNi phase abundance.

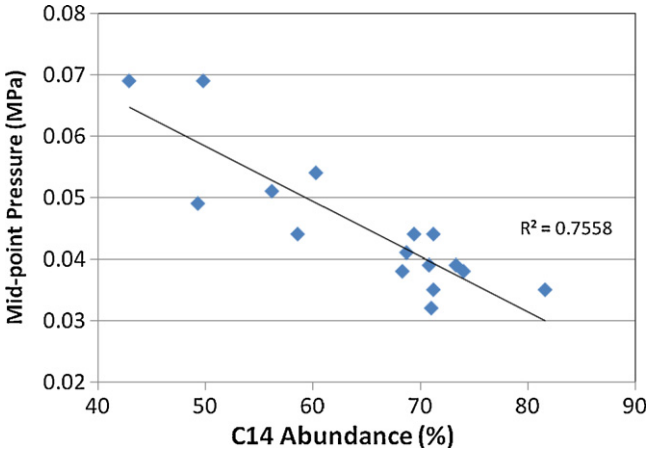

Fig. 6. Gas phase mid-point pressure from PCT analysis vs. C14 phase abundance.

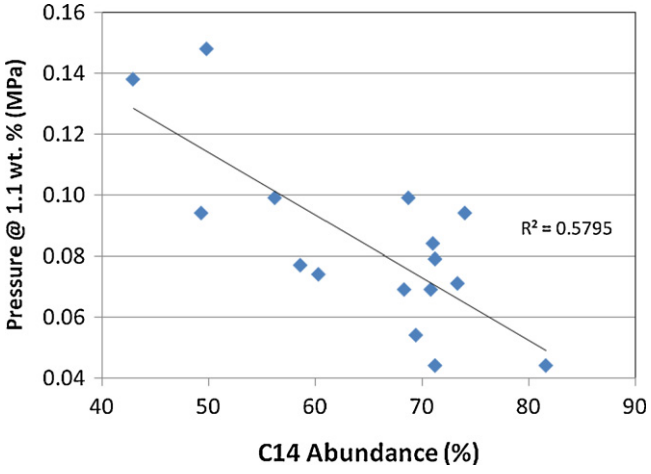

Fig. 7. Gas phase equilibrium pressure @ 1.1 wt.% storage from PCT analysis vs. C14 phase abundance.

tion. The hydrogen partial pressure in a sealed cell ranges from a few to 25 atm, which is much higher than the 1 atm of H_2 gas pressure in the bubble formed on the MH electrode during overcharge. In a fast discharge, MH electrode with a relatively lower plateau pressure will be more difficult to discharge in a sealed configuration.

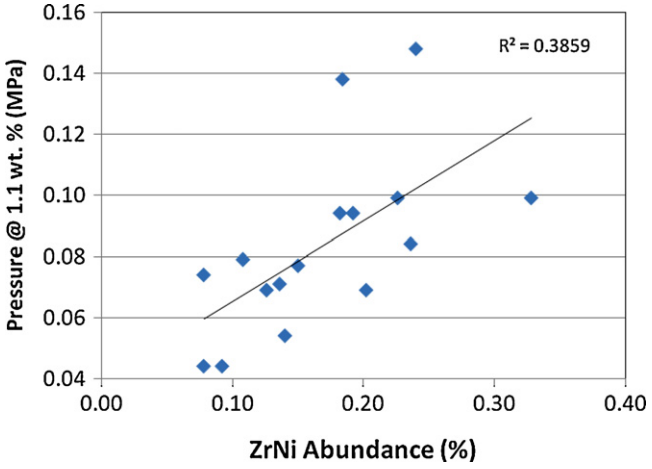

Fig. 8. Gas phase equilibrium pressure @ 1.1 wt.% storage from PCT analysis vs. ZrNi phase abundance.

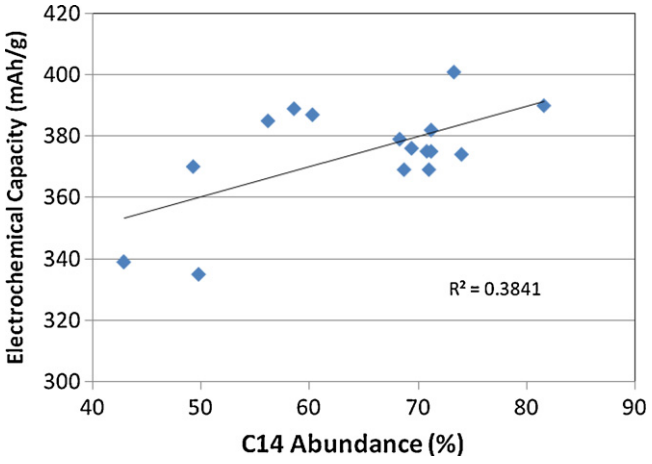

Fig. 9. Electrochemical discharge capacity measured at C/70 rate vs. C14 phase abundance.

One interesting feature can be observed from Table 2: of all the meaningful correspondences ($R^2 > 0.03$), the signs of dependency are always opposite for these three pairs—C14 vs. C15, ZrNi vs. TiNi, and Zr_7Ni_{10} vs. Zr_9Ni_{11}. The C14 vs.C15 standoff comes from the fact that they are the dominating phases and the amount of secondary phases is small and similar to each other. The ZrNi vs. TiNi standoff may originate from the same stoichiometry (AB), and the sum may be fixed considering balancing the stoichiometry of the constituent phases. In the last standoff, Zr_7Ni_{10} vs. Zr_9Ni_{11}, both phases are solidified at the same time and the sum is also fixed due to the balance of stoichiometry. The sums from the last two pairs are plotted in Fig. 12 to illustrate the small variations among the alloys.

Another finding is that in most cases C14, Zr_9Ni_{11}, and TiNi share the same sign of dependency with various properties while C15, Zr_7Ni_{10}, and ZrNi are the opposite. One possible reasoning is as following: by comparing C14, Zr_9Ni_{11}, and TiNi phase abundances vs. the additive concentration in Fig. 4a, c, and e, only Sn shows similar trends. As Sn-content increases, the abundances of those three phases decrease. In a previous study, Sn is shown to be detrimental to both charge retention and cycle life [16]. Therefore, by reducing Sn-content in the alloy, both charge retention and cycle life performance improve.

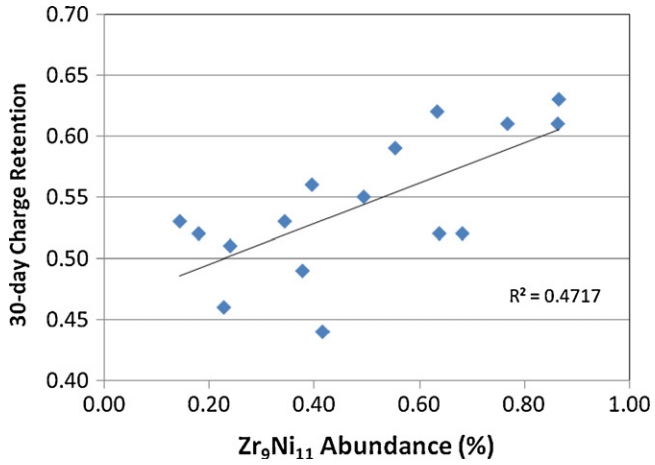

Fig. 10. 30-day charge retention in Ni/MH battery vs. Zr_9Ni_{11} phase abundance.

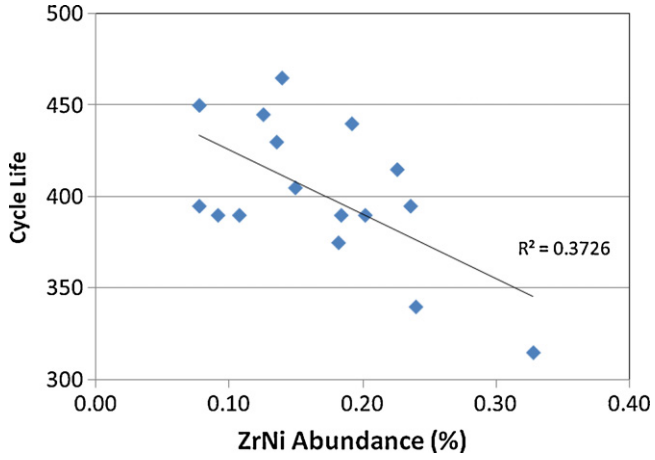

Fig. 11. Cycle life of Ni/MH battery reaching 2Ah capacity vs. ZrNi phase abundance.

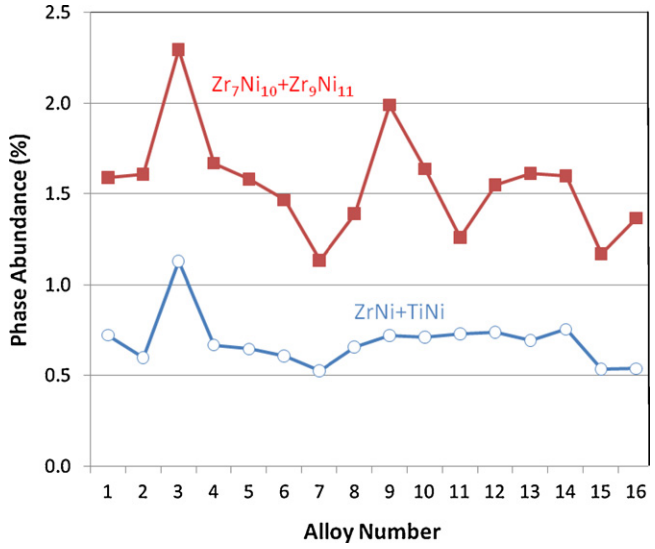

Fig. 12. The sum of Zr_7Ni_{10} and Zr_9Ni_{11} and the sum of ZrNi and TiNi phase abundances vs. the alloy number.

4. Summary

The abundance of Laves (C14 and C15) and non-Laves secondary phases (ZrNi, TiNi, Zr_7Ni_{10}, and Zr_9Ni_{11}) of 16 alloys designed by an orthogonal array with four different levels of four additives (Sn, Co, Al, and Fe) are correlated to the compositions of the alloys. The functions of the additives can be summarized as:

Sn: Promotes C15, ZrNi, and Zr_7Ni_{10} phases while suppresses C14, TiNi, and Zr_9Ni_{11} phases.
Co: Promotes C15 phase, and suppresses C14 and Zr_9Ni_{11} phases.
Al: Promotes C14 and Zr_9Ni_{11} phases, and suppresses C15 phase.
Fe: Promotes C15 and Zr_9Ni_{11} phases, and suppresses C14, ZrNi, and Zr_7Ni_{10} phases.

The phase abundances were also correlated with both the gas phase storage and electrochemical properties of the alloys. The contributions from C14, Zr_9Ni_{11}, and TiNi phases are always the opposite of those from C15, ZrNi, and Zr_7Ni_{10} phases. The first group of phases increases both the gas phase and electrochemical storage capacity, lowers the hydrogen equilibrium pressure, decreases half-cell HRD, improves both the charge retention and cycle life, and slightly decreases the capacity recovery after storing at 45 °C for 60 days.

References

[1] S.R. Ovshinsky, M.A. Fetcenko, J. Ross, Science 260 (1993) 176.
[2] M.A. Fetcenko, S.R. Ovshinsky, K. Young, B. Reichman, C. Fierro, J. Koch, F. Martin, W. Mays, T. Ouchi, B. Sommers, A. Zallen, J. Alloy Compd. 330–332 (2002) 752.
[3] M.A. Fetcenko, S.R. Ovshinsky, B. Reichman, K. Young, C. Fierro, J. Koch, A. Zallen, W. Mays, T. Ouchi, J. Power Sources 165 (2007) 544.
[4] I. Saldan, J. Frenzel, O. Shekhah, R. Chelmowski, A. Birkner, C. Wöll, J. Alloy Compd. 470 (2009) 568.
[5] S. Qiu, H. Chu, Y. Zhang, D. Sun, X. Song, L. Sun, F. Xu, J. Alloy Compd. 471 (2009) 453.
[6] M. Shibuya, J. Nakamura, H. Enoki, E. Akiba, J. Alloy Compd. 475 (2009) 543.
[7] M. Gao, H. Miao, Y. Zhao, Y. Liu, H. Pan, J. Alloy Compd. 484 (2009) 249.
[8] K. Young, M.A. Fetcenko, T. Ouchi, F. Li, J. Koch, J. Alloy Compd. 464 (2008) 238.
[9] K. Young, M.A. Fetcenko, F. Li, T. Ouchi, J. Koch, J. Alloy Compd. 468 (2009) 482.
[10] K. Young, M.A. Fetcenko, T. Ouchi, F. Li, J. Koch, J. Alloy Compd. 469 (2009) 406.
[11] K. Young, T. Ouchi, M.A. Fetcenko, J. Alloy Compd. 476 (2009) 774.
[12] K. Young, T. Ouchi, J. Koch, M.A. Fetcenko, J. Alloy Compd. 477 (2009) 749.
[13] K. Young, T. Ouchi, M.A. Fetcenko, J. Alloy Compd. 480 (2009) 428.
[14] K. Young, T. Ouchi, W. Mays, B. Reichman, M.A. Fetcenko, J. Alloy Compd. 480 (2009) 434.
[15] K. Young, T. Ouchi, M.A. Fetcenko, J. Alloy Compd. 480 (2009) 440.
[16] K. Young, M.A. Fetcenko, J. Koch, K. Morii, T. Shimizu, J. Alloy Compd. 486 (2009) 559.
[17] K. Young, T. Ouchi, B. Reichman, W. Mays, R. Regmi, G. Lawes, M.A. Fetcenko, A. Wu, J. Alloy Compd. 489 (2010) 202.
[18] K. Young, R. Regmi, G. Lawes, T. Ouchi, B. Reichman, M.A. Fetcenko, A. Wu, J. Alloy Compd. 490 (2010) 282.
[19] K. Young, J. Koch, T. Ouchi, A. Banik, M.A. Fetcenko, J. Alloy Compd. 496 (2010) 669.
[20] K. Young, M.A. Fetcenko, B. Huang, R.K. Regmi, G. Lawes, Y. Liu, J. Alloy Compd. 506 (2010) 831.
[21] K. Young, T. Ouchi, B. Huang, B. Chao, M.A. Fetcenko, L.A. Bendersky, K. Wang, C. Chiu, J. Alloy Compd. 506 (2010) 841.
[22] K. Young, T. Ouchi, B. Huang, B. Reichman, M.A. Fetcenko, J. Alloy Compd. (10-03478), submitted for publication.
[23] J.M. Joubert, M. Latroche, A. Percheron-Guégan, J. Alloy Compd. 231 (1995) 494.
[24] J.M. Joubert, M. Latroche, A. Percheron-Guégan, J. Bouet, J. Alloy Compd. 240 (1996) 219.
[25] W.K. Zhang, C.A. Ma, X.G. Yang, Y.Q. Lei, Q.D. Wang, Trans. Nonferrous Met. China 19 (1999) 505.
[26] J.M. Joubert, D. Sun, M. Latroche, A. Percheron-Guégan, J. Alloy Compd. 253–254 (1997) 564.
[27] Q.A. Zhang, Y.Q. Lei, X.G. Yang, K. Ren, Q.D. Wang, J. Alloy Compd. 292 (1999) 236.
[28] J.C. Sun, S. Li, S.J. Ji, J. Alloy Compd. 404–406 (2005) 687.
[29] F.C. Ruiz, E.B. Castro, S.G. Real, H.A. Peretti, A. Visintin, W.E. Triaca, Int. J. Hydrogen Energy 33 (2008) 3576.
[30] W.J. Boettinger, D.E. Newbury, K. Wang, L.A. Bendersky, C. Chiu, U.R. Kattner, K. Young, B. Chao, Metall. Mater. Trans. A 41 (2010) 2033.
[31] L.A. Bendersky, K. Wang, W.J. Boettinger, D.E. Newbury, K. Young, B. Chao, Metall. Mater. Trans. A 41 (2010) 1891.
[32] K. Young, T. Ouchi, M.A. Fetcenko, W. Mays, B. Reichman, Int. J. Hydrogen Energy 34 (2009) 8695.
[33] K. Young, J. Nei, B. Huang, T. Ouchi, M.A. Fetcenko, J. Alloy Compd. 501 (2010) 245.
[34] X. Song, X. Zhang, Y. Lei, Z. Zhang, Q. Wang, Int. J. Hydrogen Energy 24 (1999) 455–459.

[35] X.G. Yang, W.K. Zhang, Y.Q. Lei, Q.D. Wang, J. Electrochem. Soc. 146 (1999) 1245.
[36] Y.L. Du, X.G. Yang, Y.Q. Lei, M.S. Zhang, Int. J. Hydrogen Energy 27 (2002) 695.
[37] J. Huot, E. Akiba, T. Ogura, Y. Ishido, J. Alloy Compd. 218 (1995) 101.
[38] C. Iwakura, H. Kasuga, I. Kim, H. Inoue, M. Matsuoka, Electrochim. Acta 41 (1996) 2691.
[39] A. Visintin, H.A. Peretti, F. Ruiz, H.L. Corso, W.E. Triaca, J. Alloy Compd. 428 (2007) 244.
[40] F. Li, K. Young, T. Ouchi, M.A. Fetcenko, J. Alloy Compd. 471 (2009) 371.
[41] B.A. Talagañis, M.R. Esquivel, G. Meyer, J. Alloy Compd. 495 (2010) 541.
[42] Z. Zhou, Y. Song, S. Cui, C. Huang, W. Qian, C. Lin, Y. Zhang, Y. Lin, J. Alloy Compd. 501 (2010) 47.
[43] B.S. Chao, R.C. Young, S.R. Ovshinsky, D.A. Pawlik, B. Huang, J.S. Im, B.C. Chakoumakos, in: D. Doughty, L. Nazar, M. Arakawa, H.-P. Brack, K. Naoi (Eds.), Mater. Res. Soc. Symp. Proc., vol. 575, Warrendale, PA, 1999, p. 193.
[44] K. Young, T. Ouchi, B. Huang, J. Nei, M.A. Fetcenko, J. Alloy Compd. 501 (2010) 236.
[45] E.M. Carvalho, I.R. Harris, J. Less-Comm. Met. 106 (1985) 143.
[46] J.L. Glimois, P. Forey, J. Feron, C. Becle, J. Less-Comm. Met. 78 (1981) 45.
[47] L. Bsenko, J. Less-Comm. Met. 40 (1975) 365.
[48] W. Zhang, C. Ma, X. Yang, Y. Lei, Q. Wang, G. Li, Rare Met. Mater. Eng. 28 (1999) 202.
[49] X. Hu, J. Gu, L. Chen, G. Lu, W. Zhang, Y. Lei, Q. Wang, Chin. J. Mater. Res. 13 (1999) 129.
[50] H. Sawa, K. Ohzeki, M. Ohta, H. Nakano, S. Wakao, Z. Phys. Chem. Neue Folge 164 (1989) 1527.
[51] M.E. Badding, M.T. McCormack, D.W. Murphy, B. Vyas, US Patent 5,560,752 (1996).
[52] K. Young, T. Ouchi, Y. Liu, B. Reichman, W. Mays, M.A. Fetcenko, J. Alloy Compd. 480 (2009) 521.